

# Angle-dependent dissipation effects in topological insulator-based Josephson junctions

Ardamon Sten<sup>1,\*</sup>, Paramita Dutta<sup>2,†</sup> and Sudeep Kumar Ghosh<sup>1,‡</sup>

<sup>1</sup>*Department of Physics, Indian Institute of Technology, Kanpur 208016, India*

<sup>2</sup>*Theoretical Physics Division, Physical Research Laboratory, Navrangpura, Ahmedabad-380009, India*

(Dated: February 14, 2025)

Dissipation fundamentally alters quantum transport in Josephson junctions. Here, we demonstrate unique transport signatures in dissipative topological insulator-based Josephson junctions, which provide a powerful platform for exploring the competition between dissipation and topological protection. We incorporate dissipation effects by coupling a ‘lossy’ metallic lead at the junction to an electron reservoir, and describe its effects using an effective non-Hermitian Hamiltonian within the Lindblad formalism. Non-Hermiticity introduces finite lifetimes to the helical Andreev bound states in the junction, with imaginary energy components that depend on the quasiparticle incidence angle, while Klein tunneling remains robust for normal incidence. Unlike ‘ordinary’ non-Hermitian Josephson junctions, this system exhibits no Josephson gaps or forbidden regions, preserving topological protection. In the fully non-Hermitian regime, a tunable line of zero-energy states emerges, bounded by exceptional-like points with divergent supercurrents. Our results reveal how dissipation reshapes superconducting transport in topological insulator-based Josephson junctions, opening new directions for dissipation-engineered hybrid quantum devices.

Josephson junctions (JJs) play a pivotal role in superconducting electronics, offering a versatile tool for probing quantum transport, topological states, and unique superconducting behaviors [1]. In conventional Hermitian JJs, the superconducting phase difference determines the current-phase relationship (CPR), which is typically  $2\pi$ -periodic and sinusoidal in ‘short’ junctions [2]. These junctions are fundamental to technologies such as Superconducting Quantum Interference Devices (SQUIDs) and single-photon detectors [3]. Recent advances have revealed non-reciprocal effects, such as the Josephson diode effect, in junctions with broken inversion and time-reversal symmetries [4–7]. Topological insulator-based Josephson junctions (TIJJs) provide an ideal setting for realizing exotic quantum states [8–11], where proximity-induced superconductivity on the surface of a 3D topological insulator (3DTI) induces helical Andreev bound states (ABSs) [8, 12, 13]. These junctions support non-chiral Majorana modes [8, 14, 15], leading to  $4\pi$ -periodic Josephson effects [8, 13, 16, 17].

Dissipation is an intrinsic aspect of real-world Josephson junctions, where non-Hermitian Hamiltonians capture the effects of environmental coupling [18–23]. In non-Hermitian Josephson junctions (NH-JJs), dissipation introduces complex eigenspectra and exceptional points, leading to fundamentally different behavior from their Hermitian counterparts [18, 20, 21]. NH-JJs coupled to fermionic environments can develop phase intervals devoid of ABSs, known as Josephson gaps [18, 21]. Additionally, non-Hermitian effects modify the Josephson current and lead to novel superconducting transport phenomena [18, 20]. However, the impact of non-Hermiticity on topological Josephson junctions remains

largely unexplored, particularly in systems where dissipation competes with topological protection.

In this work, we address the central question: how does dissipation caused by coupling a ‘lossy’ metallic lead [18, 24] at the junction to an electron reservoir, affect the quantum transport properties of TIJJs? To explore this, we model the dissipative effects of the lead by an effective non-Hermitian Hamiltonian [20, 25] and investigate transport in a non-Hermitian lateral Josephson junction on the surface of a 3DTI (NH-TIJJs), as illustrated schematically in Fig. 1. Here, proximity-induced superconductivity intertwines with non-Hermitian effects, offering a unique platform to study the interplay between dissipation and topological superconductivity.

*Effective model of a NH-TIJJ:* The NH-TIJJ in Fig. 1 consists of two  $s$ -wave singlet superconductors with identical gap  $\Delta$  and phases  $\phi_L$  and  $\phi_R$  on the left and right, respectively. Dissipation due to the ‘lossy’ lead [18, 24] connected to an electron reservoir is modeled in a minimal way, within the Lindblad formalism [26, 27] (see Ap-

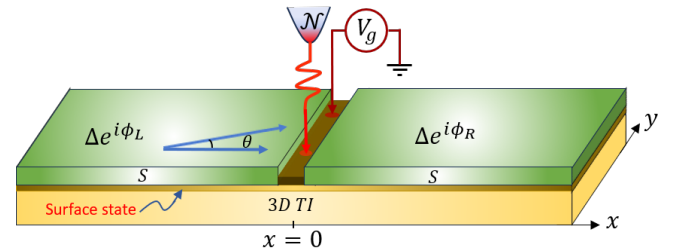


FIG. 1. **Schematic of a non-Hermitian lateral TIJJ:** A ‘short’ TIJJ formed by placing two bulk  $s$ -wave singlet superconductors on the surface of a 3DTI. A top gate and a ‘lossy’ metallic lead ( $\mathcal{N}$ ) are attached at the junction ( $x = 0$ ), where the gate modifies the potential barrier via an applied voltage  $V_g$  and the lead introduces dissipation due to coupling to an electron reservoir.

\* ardamons21@iitk.ac.in

† Jointly supervised this work; paramita@prl.res.in

‡ Jointly supervised this work; skghosh@iitk.ac.in

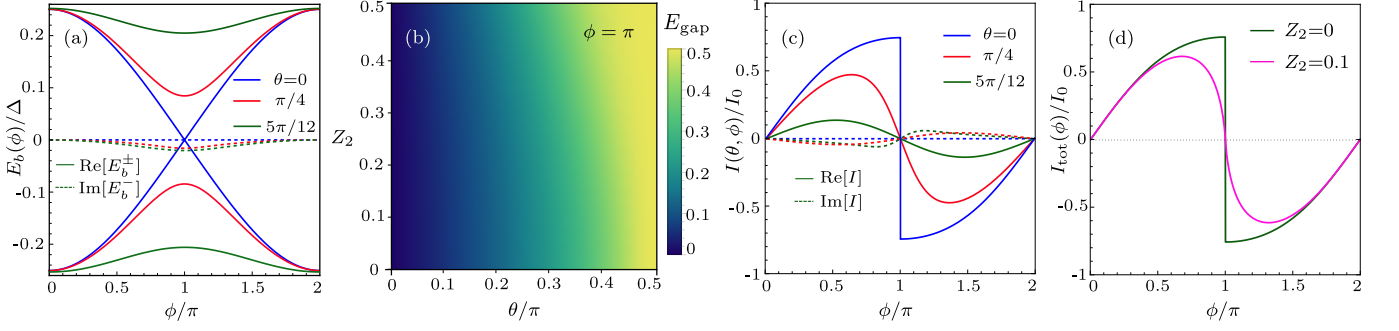


FIG. 2. **Characteristics of the NH-TIJJ for a general (complex) barrier** ( $Z_1 \neq 0, Z_2 \neq 0$ ): (a) The real (solid-lines) and imaginary (dashed-lines) parts of the ABS energy spectrum as a function of the phase difference  $\phi$  for different values of the angle of incidence  $\theta$  taking the imaginary potential barrier strength  $Z_2 = 0.1$ . (b) The variation of the energy gap in the real part of the ABS energy spectrum ( $E_{\text{gap}} = \text{Re}[E_b^{(+)} - E_b^{(-)}]$ ) at  $\phi = \pi$ . (c) The real (solid-lines) and imaginary (dashed-lines) parts of the angle-resolved supercurrent  $I(\theta, \phi)$  plotted as a function of  $\phi$  for different  $\theta$ . (d) The total supercurrent  $I_{\text{tot}}(\phi)$  as a function of  $\phi$ . We have chosen the real potential barrier strength  $Z_1 = 0.4$  and the tunneling parameter  $\gamma = 0.3$ .

pendix A for details) and neglecting quantum jumps, by an imaginary potential barrier at the junction [20]. The combined effect of the top gate and the lead is therefore captured by a complex contact junction potential barrier:  $U(x) = (V_1 - iV_2)\delta(x)$ , where  $V_1 > 0$  represents the real barrier strength tunable by the applied gate voltage  $V_g$  and  $V_2 > 0$  accounts for the imaginary barrier strength induced by the lead.

Assuming tunnel coupling between the superconductors and the 3DTI surface state [8, 12, 28, 29], the physics of the proximity-induced superconductivity on the surface state can be described by the following effective Bogoliubov-de Gennes (BdG) Hamiltonian [8, 12]:

$$\begin{aligned} \mathcal{H}_{\text{eff}} &= \Phi^\dagger H_{\text{BdG}} \Phi, \\ H_{\text{BdG}} &= \begin{bmatrix} \frac{\hbar}{i} v_F \boldsymbol{\sigma} \cdot \nabla - \mu - \Gamma(\epsilon) & \tilde{\Delta}(\epsilon) i \sigma_y e^{i\phi_{L,R}} \\ -\tilde{\Delta}(\epsilon) i \sigma_y e^{-i\phi_{L,R}} & \frac{\hbar}{i} v_F \boldsymbol{\sigma}^* \cdot \nabla + \mu - \Gamma(\epsilon) \end{bmatrix}, \\ \tilde{\Delta}(\epsilon) &= \frac{i\Gamma_0 \Delta}{\sqrt{\epsilon^2 - \Delta^2}}, \Gamma(\epsilon) = \frac{i\Gamma_0 \epsilon}{\sqrt{\epsilon^2 - \Delta^2}}, \Gamma_0 = \pi t^2 \mathcal{D}_s. \end{aligned} \quad (1)$$

Here,  $\Phi^\dagger = (\varphi_\uparrow^\dagger, \varphi_\downarrow^\dagger, \varphi_\uparrow, \varphi_\downarrow)$  is the Nambu basis and  $\varphi_s^\dagger$  is the electron creation operator with spin  $s = \uparrow, \downarrow$ .  $\mu$  is the chemical potential,  $v_F$  is the Fermi velocity of the surface states of the 3DTI and  $\sigma_i$  ( $i = 1, 2$ ) are the Pauli matrices in spin space.  $\tilde{\Delta}(\epsilon)$  is the proximity induced superconducting pairing potential which is a function of the Bogoliubov quasi-particle energy  $\epsilon$ ,  $\Gamma(\epsilon)$  is the shift in energy of the quasi-particles due to tunneling with amplitude  $t$ , and  $\Gamma_0$  is the tunneling energy scale that determines the tunneling rate.  $\mathcal{D}_s$  is the density of states of the superconductors in the normal state.

To investigate transport in the ‘short’ NH-TIJJ (Fig. 1), assuming the width of the junction much smaller than the coherence length of the superconductors, we consider  $\phi_L = 0$  and  $\phi_R = \phi$  without loss of generality. In this limit, the physics of the system can be described by [12]:

$$[H_{\text{BdG}}(\mathbf{r}) + \tau_z \sigma_0 U(x)] \Psi(\mathbf{r}) = \epsilon \Psi(\mathbf{r}), \quad (2)$$

where,  $\tau_z$  is the third Pauli matrix in the Nambu space,  $\sigma_0$  is the  $2 \times 2$  identity matrix and  $\Psi(\mathbf{r}) = [\psi_{\uparrow, \epsilon}(\mathbf{r}), \psi_{\downarrow, \epsilon}(\mathbf{r}), \psi_{\uparrow, -\epsilon}^*(\mathbf{r}), \psi_{\downarrow, -\epsilon}^*(\mathbf{r})]^T$  is the Nambu spinor wavefunction. Quasiparticles enter the barrier from the left at an angle of incidence  $\theta \in [-\pi/2, \pi/2]$  and we assume translational invariance along the  $y$ -direction. The exact shape of the barrier potential is unimportant here, as our focus is on the effects of non-Hermiticity on Klein tunneling, which remains unaffected with the change in the barrier’s form [12, 30].

*Complex helical ABSs and CPRs:* The properties of the ABSs in the NH-TIJJ can be obtained by solving Eq. (2). Since wavefunctions of the ABSs decay exponentially as  $|x| \rightarrow \infty$ , with translational invariance in the  $y$ -direction, the wavefunctions have the general form:  $\Psi(\mathbf{r}) = \sum_{k_y} \psi_{k_y}(x) e^{ik_y y}$  (see Appendix B for explicit forms of the ABS wavefunctions within the Andreev approximation). Integrating Eq. (2) around  $x = 0$  and defining  $Z = Z_1 - iZ_2$  where  $Z_{1,2} = V_{1,2}/(\hbar v_F)$  characterize the potential barrier strengths, we get the boundary condition,

$$\psi_{k_y}(0_-) = [1 + iZ\tau_z \sigma_x] \psi_{k_y}(0_+), \quad (3)$$

which leads to an equation for  $\alpha = \frac{\epsilon}{\Delta}$ :

$$\alpha(1 - \alpha) = \gamma^2 \left( \sqrt{1 - \zeta(Z, \theta) \sin^2\left(\frac{\phi}{2}\right)} - \alpha \right)^2. \quad (4)$$

Here,  $\zeta(Z, \theta) = (1 + Z^2) \cos^2(\theta) / [1 + Z^2 - \sin^2(\theta)]$  and  $\gamma = \Gamma_0/\Delta \ll 1$  is a ‘small’ dimensionless parameter characterizing the tunneling strength. We seek solutions of Eq. (4) in powers of  $\gamma$  [12]:  $|\epsilon/\Delta| = c_1 \gamma + c_2 \gamma^2 + c_3 \gamma^3$ , where  $c_1, c_2$  and  $c_3$  are unknown complex coefficients. Then in the ‘short’ junction limit, we obtain two branches (labeled by  $\pm$ ) of complex ABS spectrum with energies

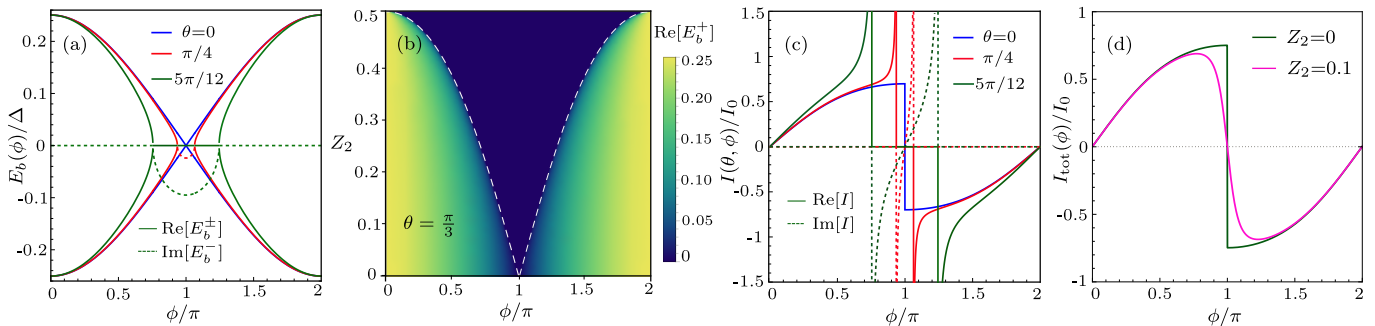


FIG. 3. **Characteristics of the NH-TIJJ for a purely dissipative barrier** ( $Z_1 = 0, Z_2 \neq 0$ ): (a) The real (solid-lines) and imaginary (dashed-lines) parts of  $E_b$  as a function of  $\phi$  for different  $\theta$  taking  $Z_2 = 0.1$ . (b) The real part of the ‘+’ branch of the ABS energy spectrum at  $\theta = \pi/3$ . The blue region shows zero-energy states (ZES) and the change in its boundary demonstrates tuning of the line of ZES (dotted line corresponding to the analytical expression in Eq. (9)) by the non-Hermiticity strength  $Z_2$ . (c) The real (solid-lines) and imaginary (dashed-lines) parts of  $I(\theta, \phi)$  as a function of  $\phi$  for different  $\theta$ . (d) Total supercurrent  $I_{\text{tot}}(\phi)$  as a function of  $\phi$  for the fully transparent ( $Z_2=0$ ) and purely non-Hermitian ( $Z_2=0.1$ ) cases.

(see Appendix B for details):

$$\frac{E_b^{(\pm)}(\phi)}{\Delta} = \pm \left[ (\gamma - \gamma^2 + \gamma^3) \left\{ 1 - \zeta(Z, \theta) \sin^2 \left( \frac{\phi}{2} \right) \right\}^{\frac{1}{2}} + \frac{\gamma^3}{2} \left\{ 1 - \zeta(Z, \theta) \sin^2 \left( \frac{\phi}{2} \right) \right\}^{\frac{3}{2}} \right]. \quad (5)$$

The real parts of  $E_b^{(\pm)}$  represent physical energies of the ABSs while the imaginary part of  $E_b^{(-)}$  represents their finite lifetime [20, 31]. The variation of the ABS spectrum with changing  $\theta$  is shown in Fig. 2(a). For normal incidence ( $\theta = 0$ ), since  $\zeta$  becomes independent of  $Z$ , the ABS spectra is gapless exhibiting a zero-energy crossing at  $\phi = \pi$  and lack any imaginary components. This indicates no dissipation for normally incident quasiparticles preserving topological protection of the Klein tunneling effect [32] in 3DTI surface states [33–35]. In contrast, obliquely incident quasiparticles experience the effect of non-Hermiticity, resulting in two qualitatively new effects: finite lifetime for ABSs and a fully gapped ABS spectrum. The energy gap,  $E_{\text{gap}}(\phi) = \text{Re}[E_b^{(+)}(\phi) - E_b^{(-)}(\phi)]$ , varies with  $\theta$  and  $Z_i$ , as shown in Fig. 2(b).

The angle-resolved Josephson current  $I(\theta, \phi)$  at zero temperature is calculated using the occupied part of the ABS spectrum with the formula [36, 37]:

$$I(\theta, \phi) = \frac{2e}{\hbar} \frac{dE_b^{(-)}}{d\phi}, \quad (6)$$

which for the NH-TIJJ gives,

$$\frac{I(\theta, \phi)}{I_0} = \frac{\zeta \left[ 1 - \gamma + \frac{5}{2}\gamma^2 - \frac{3}{2}\gamma^2\zeta \sin^2 \left( \frac{\phi}{2} \right) \right]}{\left[ 1 - \zeta \sin^2 \left( \frac{\phi}{2} \right) \right]^{1/2}} \sin(\phi). \quad (7)$$

Here,  $I_0 = eN\Gamma_0/(2\hbar)$  with  $N$  being the number of transmission channels. The variation of  $I(\theta, \phi)$  for different  $\theta$

is shown in Fig. 2(c). For normal incidence,  $I(\theta, \phi)$  is always real as expected,  $2\pi$ -periodic and changes sign abruptly at  $\phi = \pi$  due to the change in the ground state occupation at the zero-energy crossing (see Fig. 2(a)) [38–40]. On the other hand, for oblique incidence ( $\theta \neq 0$ ),  $I(\theta, \phi)$  becomes non-sinusoidal and complex. The magnitude of the real component decreases with increasing  $\theta$  while the imaginary component increases, indicating that the effect of non-Hermiticity is more effective with increasing  $\theta$ .

The total equilibrium Josephson current ( $I_{\text{tot}}$ ) is obtained as:

$$I_{\text{tot}}(\phi) = \int_{-\pi/2}^{\pi/2} I(\phi, \theta) \cos(\theta) d\theta. \quad (8)$$

Then the CPR for the NH-TIJJ is shown in Fig. 2(d). We note that the  $2\pi$ -periodic CPR for the Hermitian case ( $Z_2 = 0$ ) that changes sign discontinuously at  $\phi = \pi$  transforms into a non-sinusoidal CPR that changes sign smoothly at  $\phi = \pi$  for the non-Hermitian case ( $Z_2 = 0.1$ ).

*Purely dissipative barrier:* In order to demonstrate the sole effect of the imaginary potential barrier, we consider the  $Z_1 = 0$  case which is the non-Hermitian counterpart of the Kulik-Omel’yanchuk limit with fully transparent barrier [41]. The corresponding ABS energy spectrum is shown in Fig. 3(a) for different  $\theta$ . To compare, we note that in the purely Hermitian case ( $Z_2 = 0, Z_1 \neq 0$ ), the ABS spectrum has a zero-energy crossing at  $\phi = \pi$  at  $\theta = 0$  and it changes from gapless to gapped for larger  $\theta$  [12]. In contrast, for this purely non-Hermitian case, the ABS spectrum *always* remains gapless and the zero-energy crossing at  $\phi = \pi$  for  $\theta = 0$  evolves into a line of ZES on the  $\phi$ -axis for any  $\theta \neq 0$ . The ZES also have a non-zero imaginary energy component indicating their finite lifetime. The boundary of the ZES-line is determined by the condition:  $\zeta(Z_2, \theta) \sin^2(\phi/2) = 1$  giving the position of the boundary as:

$$\phi_n(Z_2, \theta) = 2n\pi \pm 2 \sin^{-1} \left( 1/\sqrt{\zeta(Z_2, \theta)} \right), \quad (9)$$

where,  $n$  is an integer. These boundary points mimic the behavior of exceptional points usually observed in non-Hermitian systems [22, 42] and are tunable by  $Z_2$  and  $\theta$ , as shown in Fig. 3(b). The blue region indicates the ZES and its boundary given by Eq. (9) characterizes the location of the exceptional-like points that widens as  $Z_2$  increases, indicating that the strength of non-Hermiticity is directly responsible for the formation and tuning of the positions of these points (see also Appendix B for more details). However, for normal incidence we see that the spectrum (Fig. 3(a)) remains the same as in the Hermitian case and there is no formation of the exceptional-like points. This is expected since for normal incidence the effect of non-Hermiticity is not felt by the quasiparticles due to Klein tunneling, as discussed earlier.

To analyze the nature of the ZES further, we note that their wavefunctions for  $\phi = (2n+1)\pi$ , with  $n$  being an integer, are (see Appendix B):  $\Sigma_{\pm}(x, \theta) = \chi_{\pm}(\theta)e^{\pm ik_F x - x/\xi}$  with  $\chi_{\pm}(\theta) = (1, \pm e^{\pm i\theta}, -ie^{\pm i\theta}, \pm i)^T$ . These two wavefunctions are orthogonal to each other which prevents mixing of two zero energy ABSs. For normal incidence, they are also time reversal partners of each other as they are connected by the time reversal symmetry operation as  $\Sigma_-(x, 0) = \tau_0 i \sigma_y \Sigma_+(x, 0)$  [12] but this is not the case for a general  $\theta \neq 0$ . Hence, for  $\theta = 0$ , the ZES are indeed Majorana zero modes protected by time-reversal symmetry [8] but for general  $\theta \neq 0$ , they are not Majorana modes.

The angle-resolved Josephson supercurrent in Eq. (7) diverges at the exceptional-like points as shown in Fig. 3(c) similar to other NH-JJs where non-Hermiticity is introduced within the superconductor Hamiltonian [19] or through the self-energy term [18, 22]. Hence, we compute the total physical Josephson current in Eq. (8) by excluding the exceptional-like points avoiding the divergences. The corresponding CPR is shown in Fig. 3(d). We note that the  $2\pi$ -periodic CPR for the fully transparent junction (green) becomes non-sinusoidal for this purely non-Hermitian (pink) case and the magnitude of the critical current also decreases.

*Comparison with ‘ordinary’ NH-JJs:* We consider an ‘ordinary’ lateral NH-JJ, where the 3DTI in Fig. 1 is replaced by an ‘ordinary’ metal, to highlight the special features of the NH-TIJJ. Proceeding in a similar way, in the ‘short’ junction limit within the Andreev approximation, the ABS energies are given by (see Appendix C for details),

$$g_2(\theta, \phi) \left( \frac{E_b}{\Delta'} \right)^2 = g_1(\theta, \phi) Z^2 + \cos^4(\theta) \cos^2 \left( \frac{\phi}{2} \right) + 2Z_1^2 \cos^2(\theta) \pm 2Z_2 \sqrt{g_1(\theta, \phi) \cos^2 \left( \frac{\phi}{2} \right) - Z_1^2}. \quad (10)$$

Here,  $Z^2 = (Z_1^2 + Z_2^2)$  with the dimensionless barrier parameters defined as  $Z_i = \frac{mV_i}{\hbar^2 k_F}$  in this case,  $g_1(\theta, \phi) = Z^2 - \cos^2(\theta) \sin^2 \left( \frac{\phi}{2} \right)$ ,  $g_2(\theta, \phi) =$

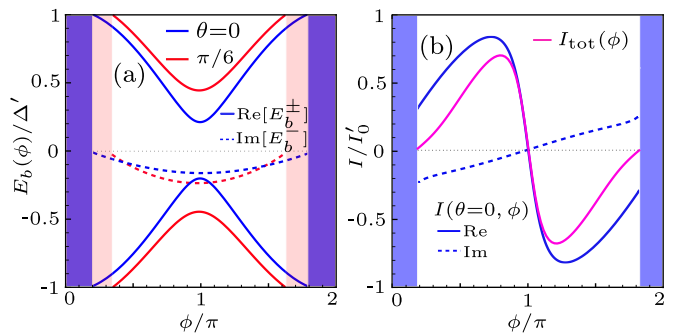


FIG. 4. **Characteristics of an ‘ordinary’ NH-JJ:** (a) The ABS spectrum of an ‘ordinary’ NH-JJ (the 3DTI in Fig. 1 is replaced by a metal) for different  $\theta$ . (b) Variation of the complex angle-resolved supercurrent for  $\theta = 0$ , and the CPR of the junction. Here,  $I'_0 = Ne\Delta'/\hbar$  and  $Z_1 = Z_2 = 0.2$ . The shaded regions indicate the Josephson gaps.

$[Z^2 + \cos^2(\theta)]^2 - 4Z_2^2 \cos^2(\theta)$  and  $\Delta'$  is the induced superconducting gap amplitude in the metal. We note that the ABS solutions exist *only* in the allowed regime:  $\phi \in [\phi_l, \phi_u]$  in contrast to the NH-TIJJ case. Furthermore, the ABSs decay exponentially with a decay length  $\lambda = \frac{\hbar v_F}{\Delta'} (1 - E_b^2/\Delta^2)^{-1/2}$ , which sets the condition for their existence:  $\text{Re}[\lambda] > 0$ . This condition results in Josephson gaps, defined as intervals in  $\phi$  where there are no ABS solutions. The phase boundaries of the Josephson gaps [20] are given by:  $\phi_l = 2n\pi + \phi_0(Z)$  and  $\phi_u = (2n+1)\pi - \phi_0(Z)$  where  $\phi_0(Z) = 2 \sin^{-1} \left( \frac{\sqrt{2}Z_2}{\sqrt{\cos^2(\theta) + Z^2}} \right)$  with  $n$  being an integer.

The ABS spectra for  $\theta = 0$  and a finite  $\theta = \pi/6$  are shown in Fig. 4(a). The spectra is complex, with both the energy gap between the real branches and the behavior of the imaginary part strongly dependent on the angle of incidence.  $\text{Im}[E_b^{(-)}]$  increases with increasing  $\theta$  which indicates that the effect of non-Hermiticity increases with increasing  $\theta$  consistent with the NH-TIJJ case (Fig. 2). The boundary of the Josephson gaps (shaded regions in Fig. 4) also increases with increasing  $\theta$  which demonstrates non-Hermiticity effect is controlled both by the imaginary potential strength  $Z_2$  and  $\theta$ . Hence, the key differences between the ABS spectra of this ‘ordinary’ NH-JJ and the previously described NH-TIJJ are: (1) the presence of Josephson gaps in the NH-JJ, which are absent in the NH-TIJJ, and (2) the absence of zero-energy states in the NH-JJ, which were present in the NH-TIJJ.

The variation of the real and imaginary parts of the the angle-resolved Josephson current  $I(\theta, \phi)$  in Eq. (6) for normal incidence is shown in Fig. 4(b). We note that the absence of any Josephson current within the Josephson gaps as expected since there are no ABS solutions within these gaps. The total Josephson current ( $I_{\text{tot}}$ ) also shown in Fig. 4(d) demonstrates that the CPR is non-sinusoidal and exhibits a Josephson gap same as that of the  $\theta = 0$  case in Fig. 4(a). This is in stark contrast with the CPR for the NH-TIJJ case (shown in Fig. 3(d)), which exhibits



no Josephson gaps.

*Summary and outlook:* We have investigated the quantum transport properties of a dissipative Josephson junction on the surface of a 3DTI, aiming to elucidate the interplay between dissipation and topological protection. Dissipation, modeled via an effective non-Hermitian Hamiltonian within the Lindblad formalism, arises from coupling to a ‘lossy’ metallic lead [18, 24] at the junction to an electron reservoir. Our study reveals that the Andreev bound state (ABS) spectrum is generally complex for oblique incidence, indicating their finite lifetimes and decoherence in Cooper pair transport due to non-Hermiticity in this NH-TIJJ. Notably, normally incident quasiparticles preserve Klein tunneling, maintaining a real gapless ABS spectrum. Unlike ‘ordinary’ NH-JJs, NH-TIJJs lack Josephson gaps, highlighting their topological protection. Moreover, in the purely non-Hermitian regime, a tunable line of ZES emerges along the phase difference axis, with boundary points exhibiting exceptional-point-like features such as divergent angle-resolved supercurrents. Non-Hermiticity also reshapes the CPR, transforming it from a discontinuous  $2\pi$ -periodic form into a smoothly varying, non-sinusoidal function while preserving  $2\pi$ -periodicity.

The physics of the ‘short’ NH-TIJJ described in this paper can be realized in practical devices, such as Nb-superconductors on the surface of a HgTe 3DTI [43], with dissipation introduced by attaching a ‘lossy’ metallic lead [18, 24] at the junction. For such a setup, relevant parameters include  $\Delta \simeq 1$  meV,  $\Gamma_0 \simeq 0.2$  meV,  $\hbar v_F \simeq 250 - 350$  meV-nm and the junction width  $< 1.25 - 1.75$   $\mu\text{m}$  [43]. Another promising platform is Nb-Bi<sub>2</sub>Te<sub>3</sub>-Nb JJs [44, 45]. Our findings thus highlight the intricate interplay between topology, superconductivity, and dissipation, providing critical insights into the experimental realization of dissipation-engineered hybrid quantum devices and paving the way for leveraging non-Hermitian effects in TIJJs to advance quantum computing architectures.

### Acknowledgments

A.S. acknowledges the hospitality of PRL, Ahmedabad, during this work and thanks Amartya Pal for valuable discussions. P.D. acknowledges Department of Space (DoS), India for all the support at PRL, Ahmedabad and, the hospitality at IIT Kanpur during this work. S.K.G. acknowledges financial support from IIT Kanpur via the Initiation Grant (IITK/PHY/2022116). P.D. and S.K.G. also acknowledge Anusandhan National Research Foundation (ANRF) erstwhile Science and Engineering Research Board (SERB), India for financial support through the Start-up Research Grants: SRG/2022/001121 and SRG/2023/000934 respectively.

### Appendix A: Lindblad formalism to describe dissipation due to the normal lead

To investigate the impact of coupling a ‘lossy’ metallic lead at the junction to an electron reservoir on the transport properties of a TIJJ, we model the system as an open quantum system interacting with its environment, following Ref. [20]. The total Hamiltonian can be decomposed as  $H = H_0 + H_E + H_c$ , where  $H_0$  is the system Hamiltonian,  $H_E$  describes the environment, and  $H_c$  represents the coupling between the system and environment. The dissipative dynamics induced by this coupling term can be described by the Lindblad master equation [26, 27, 46, 47]:

$$\frac{d\rho_0}{dt} = -i[H_0, \rho_0] + \sum_m \eta \left( \hat{\mathcal{L}}_m \rho_0 \hat{\mathcal{L}}_m^\dagger - \frac{1}{2} \{ \hat{\mathcal{L}}_m \hat{\mathcal{L}}_m^\dagger, \rho_0 \} \right). \quad (\text{A1})$$

Here,  $\rho_0$  is the reduced density matrix of the system,  $\hat{\mathcal{L}}_m$  is the Lindblad (quantum jump) operator, and  $\eta > 0$  is the dissipation rate. Rearranging this equation yields:

$$\frac{d\rho_0}{dt} = -i(H_{\text{eff}}\rho_0 - \rho_0 H_{\text{eff}}^\dagger) + \sum_m \eta \hat{\mathcal{L}}_m \rho_0 \hat{\mathcal{L}}_m^\dagger, \quad (\text{A2})$$

where, the effective Hamiltonian is

$$H_{\text{eff}} = H_0 - \frac{i}{2} \sum_m \eta \hat{\mathcal{L}}_m \hat{\mathcal{L}}_m^\dagger. \quad (\text{A3})$$

The non-Hermitian term  $-\frac{i}{2} \sum_m \eta \hat{\mathcal{L}}_m \hat{\mathcal{L}}_m^\dagger$  accounts for the ‘loss’ due to coupling with the environment. By neglecting quantum jumps in the second term on the right-hand side of Eq. (A2), the system’s dynamics can be effectively described by  $H_{\text{eff}}$  [20, 25]. This motivates modeling the non-Hermiticity introduced by the ‘lossy’ lead in the TIJJ by an imaginary potential term  $-iV_2$  where  $V_2 > 0$  is real.

### Appendix B: Wavefunctions and bound states for NH-TIJJs

The wavefunctions for the two regions  $x < 0$  ( $x_-$ ) and  $x > 0$  ( $x_+$ ) of the NH-TIJJ, within the Andreev approximation and considering the limit of large Fermi energy ( $\mu \gg \tilde{\Delta}(\epsilon)$ ), obtained by solving Eq. (2) have the

forms [12],

$$\psi_{k_y}(x_+) = A \begin{bmatrix} 1 \\ e^{i\theta} \\ -e^{i\theta} a_R^+ \\ a_R^+ \end{bmatrix} e^{ik_F x \cos(\theta) - x/\xi} + B \begin{bmatrix} 1 \\ -e^{-i\theta} \\ e^{-i\theta} a_R^- \\ a_R^- \end{bmatrix} e^{-ik_F x \cos(\theta) - x/\xi}, \quad (\text{B1})$$

$$\psi_{k_y}(x_-) = C \begin{bmatrix} 1 \\ e^{i\theta} \\ -e^{i\theta} a_L^- \\ a_L^- \end{bmatrix} e^{ik_F x \cos(\theta) + x/\xi} + D \begin{bmatrix} 1 \\ -e^{-i\theta} \\ e^{-i\theta} a_L^+ \\ a_L^+ \end{bmatrix} e^{-ik_F x \cos(\theta) + x/\xi}, \quad (\text{B2})$$

where,  $A$ ,  $B$ ,  $C$  and  $D$  are constants, and  $k_F$  is the Fermi wavevector. The Andreev reflection amplitudes for the electron-like (+) and hole-like (-) quasiparticles are,

$$a_{L,R}^\pm(\epsilon) = \frac{\tilde{\Delta}(\epsilon) e^{-i\phi_{L,R}}}{\mathcal{E}(\epsilon) \pm i\sqrt{\tilde{\Delta}^2(\epsilon) - \mathcal{E}^2(\epsilon)}}, \quad (\text{B3})$$

$$\cos(\theta) = \sqrt{1 - \left(\frac{k_y}{k_F}\right)^2}, \quad \mathcal{E}(\epsilon) = \epsilon + i\Gamma(\epsilon). \quad (\text{B4})$$

Inserting Eqs. (B1) and (B2) in Eq. (3), we get a set of four equations for  $A$ ,  $B$ ,  $C$  and  $D$ . For non-trivial solutions, the determinant of the coefficients of this system of equations must vanish leading to the following equation for the ABS energy:

$$[a_L^+ - a_L^-][a_R^+ - a_R^-] = \zeta(Z, \theta)[a_R^+ - a_L^+][a_L^- - a_R^-]. \quad (\text{B5})$$

Substituting the coefficients from Eq. (B3) in Eq. (B5) we obtain the following equation which can be rearranged to get Eq. (4),

$$\left(\frac{\epsilon}{\Delta} + \frac{\epsilon}{\Gamma_0} \sqrt{1 - \frac{\epsilon^2}{\Delta^2}}\right)^2 = 1 - \zeta(Z, \theta) \sin^2\left(\frac{\phi}{2}\right). \quad (\text{B6})$$

Substituting the form:  $|\epsilon/\Delta| = c_1\gamma + c_2\gamma^2 + c_3\gamma^3$ , in Eq. (4) and equating the coefficients of different powers in  $\gamma$ , we obtain

$$\begin{aligned} c_1 &= -c_2 = \left[1 - \zeta(Z, \theta) \sin^2\left(\frac{\phi}{2}\right)\right]^{\frac{1}{2}}, \\ c_3 &= \left[1 - \zeta(Z, \theta) \sin^2\left(\frac{\phi}{2}\right)\right]^{\frac{1}{2}} \\ &+ \frac{1}{2} \left[1 - \zeta(Z, \theta) \sin^2\left(\frac{\phi}{2}\right)\right]^{\frac{3}{2}}. \end{aligned} \quad (\text{B7})$$

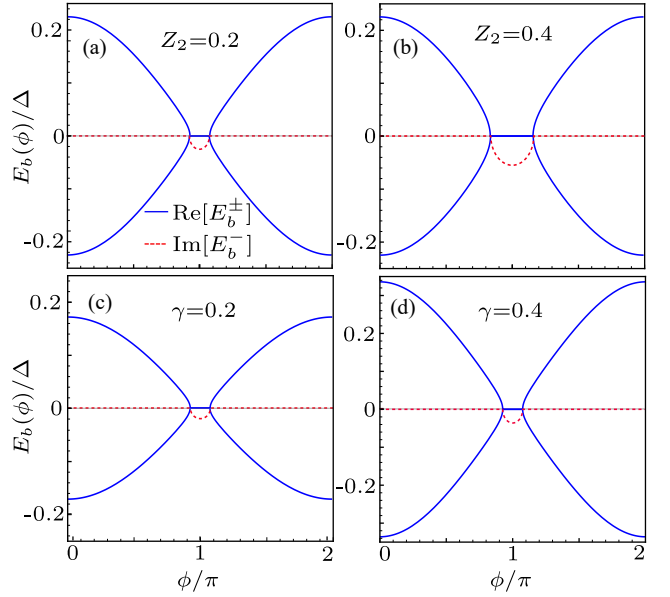


FIG. 5. **ABS energy for purely non-Hermitian TIJJ** ( $Z_1 = 0$ ,  $\theta = \pi/6$ ): The complex ABS energy plotted for two different values of  $Z_2$  in (a) and (b) taking  $\gamma = 0.3$ , and for two different values of  $\gamma$  in (c) and (d) keeping  $Z_2 = 0.1$ .

For the purely non-Hermitian case ( $Z_1 = 0$ ,  $Z_2 \neq 0$ ), the variation of the ABS energies in this NH-TIJJ for different values of  $Z_2$  and  $\gamma$  is illustrated in Fig. 5. Fig. 5(a) and (b) show that the imaginary component of the ABS energy increases with increasing  $Z_2$ . Hence, as the strength of non-Hermiticity grows, the lifetime of the ABS quasiparticles in the junction decreases, leading to greater decoherence in charge transport. Furthermore, the length of the zero-energy line increases with  $Z_2$ , indicating that non-Hermiticity directly facilitates the formation of these ZES. The variation of the ABS energy with  $\gamma$  in this regime is shown in Fig. 5(c) and (d). Increasing  $\gamma$  raises the maximum energy of the bound states, as enhanced tunneling allows more quasiparticles to traverse from the superconducting regions into the junction, resulting in a larger number of bound states. However, the zero-energy line remains unaffected by changes in  $\gamma$ .

### Appendix C: Hamiltonian and bound states for an ‘ordinary’ NH-JJ

The BdG Hamiltonian for the ‘ordinary’ NH-JJ (3DTI in Fig. 1 is replaced by a 3D metal), in the same way as Eq. (2) in the main text, can be written as,

$$H_{\text{BdG}}^{(0)} = \begin{bmatrix} \hat{h}_0 - \mu + U(x) & \Delta' e^{i\phi_{L,R}} \\ \Delta' e^{-i\phi_{L,R}} & -(\hat{h}_0 - \mu + U^*(x)) \end{bmatrix} \quad (\text{C1})$$

Here,  $\hat{h}_0 = -\frac{\hbar^2}{2m}(\partial_x^2 + \partial_y^2)$  is the kinetic energy operator,  $m$  is the mass of electron,  $\mu$  is the chemical potential of the superconductor and  $U(x)$  is the complex potential

barrier. The induced pair potential  $\Delta'$  is assumed to be energy independent.

The wavefunctions for the bound states are obtained by solving for the eigenstates of  $H_{\text{BdG}}^{(0)}$  in Eq. (C1). Within the Andreev approximation ( $k_h = k_e^* \simeq k_F$ ) and taking  $p_y$  is a good quantum number, the general forms of the wavefunctions are given by:  $\Psi(\mathbf{r}) = \sum_{k_y} \psi_{k_y}(x) e^{ik_y y}$ , where,

$$\begin{aligned} \psi_{k_y}(x_-) &= A_1 e^{ik_h x \cos(\theta)} \begin{pmatrix} v \\ u \end{pmatrix} + B_1 e^{-ik_e x \cos(\theta)} \begin{pmatrix} u \\ v \end{pmatrix}, \\ \psi_{k_y}(x_+) &= C_1 e^{ik_e x \cos(\theta)} \begin{pmatrix} u e^{\frac{i\phi}{2}} \\ v e^{-\frac{i\phi}{2}} \end{pmatrix} \\ &+ D_1 e^{-ik_h x \cos(\theta)} \begin{pmatrix} v e^{\frac{i\phi}{2}} \\ u e^{-\frac{i\phi}{2}} \end{pmatrix}, \\ u &= \sqrt{\frac{1}{2} \left( 1 + \frac{i\sqrt{\Delta'^2 - \epsilon^2}}{\epsilon} \right)}, \\ v &= \sqrt{\frac{1}{2} \left( 1 - \frac{i\sqrt{\Delta'^2 - \epsilon^2}}{\epsilon} \right)}, \end{aligned}$$

where,  $\cos(\theta) = \sqrt{1 - (k_y/k_F)^2}$ . The boundary conditions for the wavefunctions on either side of the junctions are,

$$\begin{aligned} \Psi_-(0) &= \Psi_+(0), \\ \Psi'_+(0) - \Psi'_-(0) &= -\frac{2m}{\hbar^2} (iV_1\tau_0 + V_2\tau_z) \Psi(0). \end{aligned} \quad (\text{C2})$$

The boundary conditions in Eq. (C2) lead to four sets of equations for the amplitudes  $A_1$ ,  $B_1$ ,  $C_1$  and  $D_1$ . For a non-trivial solution the determinant of the characteristic equation must be zero from which we obtain the secular equation to determine the ABS energy to be,

$$\begin{aligned} \frac{\Delta'^2}{\epsilon^2} (Z^2 + \cos^2(\theta) \cos^2(\phi/2)) \\ - 2iZ_2 \cos(\theta) \sqrt{\frac{\Delta'^2}{\epsilon^2} - 1} - (Z^2 + \cos^2(\theta)) = 0. \end{aligned} \quad (\text{C3})$$

Solving the above Eq. (C3) for  $y = \epsilon^2/\Delta'^2$ , we obtain the expression of ABS energy in Eq. (10).

- [1] E. L. Wolf, G. B. Arnold, M. A. Gurvitch, and J. F. Zasadzinski, *Josephson junctions: history, devices, and applications* (CRC Press, 2017).
- [2] B. D. Josephson, The discovery of tunnelling supercurrents, *Rev. Mod. Phys.* **46**, 251 (1974).
- [3] E. D. Walsh, W. Jung, G.-H. Lee, D. K. Efetov, B.-I. Wu, K.-F. Huang, T. A. Ohki, T. Taniguchi, K. Watanabe, P. Kim, D. Englund, and K. C. Fong, Josephson junction infrared single-photon detector, *Science* **372**, 409 (2021).
- [4] C. Baumgartner, L. Fuchs, A. Costa, S. Reinhardt, S. Gronin, G. C. Gardner, T. Lindemann, M. J. Manfra,

- P. E. Faria Junior, D. Kochan, *et al.*, Supercurrent rectification and magnetochiral effects in symmetric josephson junctions, *Nature nanotechnology* **17**, 39 (2022).
- [5] B. Pal, A. Chakraborty, P. K. Sivakumar, M. Davydova, A. K. Gopi, A. K. Pandeya, J. A. Krieger, Y. Zhang, M. Date, S. Ju, *et al.*, Josephson diode effect from cooper pair momentum in a topological semimetal, *Nature physics* **18**, 1228 (2022).
- [6] F. Ando, Y. Miyasaka, T. Li, J. Ishizuka, T. Arakawa, Y. Shiota, T. Moriyama, Y. Yanase, and T. Ono, Observation of superconducting diode effect, *Nature* **584**, 373 (2020).
- [7] D. Debnath and P. Dutta, Gate-tunable josephson diode effect in rashba spin-orbit coupled quantum dot junctions, *Phys. Rev. B* **109**, 174511 (2024).
- [8] L. Fu and C. L. Kane, Superconducting proximity effect and majorana fermions at the surface of a topological insulator, *Phys. Rev. Lett.* **100**, 096407 (2008).
- [9] J. Cayao, P. Dutta, P. Bureset, and A. M. Black-Schaffer, Phase-tunable electron transport assisted by odd-frequency cooper pairs in topological josephson junctions, *Phys. Rev. B* **106**, L100502 (2022).
- [10] P. Dutta, Phase-dependent charge and heat current in thermally biased short josephson junctions formed at helical edge states, *New Journal of Physics* **25**, 083024 (2023).
- [11] P. Dutta, J. Cayao, A. M. Black-Schaffer, and P. Bureset, Nonlocality of majorana bound states revealed by electron waiting times in a topological andreev interferometer, *Phys. Rev. Res.* **6**, L012062 (2024).
- [12] G. Tkachov and E. M. Hankiewicz, Helical andreev bound states and superconducting klein tunneling in topological insulator josephson junctions, *Phys. Rev. B* **88**, 075401 (2013).
- [13] C. T. Olund and E. Zhao, Current-phase relation for josephson effect through helical metal, *Phys. Rev. B* **86**, 214515 (2012).
- [14] M. Z. Hasan and C. L. Kane, Colloquium: Topological insulators, *Rev. Mod. Phys.* **82**, 3045 (2010).
- [15] X.-L. Qi and S.-C. Zhang, Topological insulators and superconductors, *Rev. Mod. Phys.* **83**, 1057 (2011).
- [16] L. Fu and C. L. Kane, Josephson current and noise at a superconductor/quantum-spin-hall-insulator/superconductor junction, *Phys. Rev. B* **79**, 161408 (2009).
- [17] J. Wiedenmann, E. Bocquillon, R. S. Deacon, S. Hartinger, O. Herrmann, T. M. Klapwijk, L. Maier, C. Ames, C. Brüne, C. Gould, *et al.*, 4  $\pi$ -periodic josephson supercurrent in hgte-based topological josephson junctions, *Nature communications* **7**, 10303 (2016).
- [18] J. Cayao and M. Sato, Non-hermitian phase-biased josephson junctions, *Phys. Rev. B* **110**, L201403 (2024).
- [19] V. Kornich, Current-voltage characteristics of the normal metal-insulator-pt-symmetric non-hermitian superconductor junction as a probe of non-hermitian formalisms, *Phys. Rev. Lett.* **131**, 116001 (2023).
- [20] C.-A. Li, H.-P. Sun, and B. Trauzettel, Anomalous andreev spectrum and transport in non-hermitian josephson junctions, *Phys. Rev. B* **109**, 214514 (2024).
- [21] P.-X. Shen, Z. Lu, J. L. Lado, and M. Trif, Non-hermitian fermi-dirac distribution in persistent current transport, *Phys. Rev. Lett.* **133**, 086301 (2024).
- [22] J. Cayao and M. Sato, Non-hermitian multiterminal phase-biased josephson junctions, *Phys. Rev. B* **110**,

- 235426 (2024).
- [23] C. W. J. Beenakker, Josephson effect in a junction coupled to an electron reservoir, *Applied Physics Letters* **125**, 122601 (2024).
- [24] D. C. Ohnmacht, V. Wilhelm, H. Weisbrich, and W. Belzig, Non-hermitian topology in multiterminal superconducting junctions, arXiv preprint arXiv:2408.01289 (2024).
- [25] P. M. Harrington, E. J. Mueller, and K. W. Murch, Engineered dissipation for quantum information science, *Nature Reviews Physics* **4**, 660 (2022).
- [26] H.-P. Breuer and F. Petruccione, *The theory of open quantum systems* (Oxford University Press, USA, 2002).
- [27] A. J. Daley, Quantum trajectories and open many-body quantum systems, *Advances in Physics* **63**, 77 (2014).
- [28] A. C. Potter and P. A. Lee, Engineering a  $p+ip$  superconductor: Comparison of topological insulator and rashba spin-orbit-coupled materials, *Phys. Rev. B* **83**, 184520 (2011).
- [29] M. Lababidi and E. Zhao, Microscopic simulation of superconductor/topological insulator proximity structures, *Phys. Rev. B* **83**, 184511 (2011).
- [30] G. Tkachov and E. M. Hankiewicz, Spin-helical transport in normal and superconducting topological insulators, *physica status solidi (b)* **250**, 215 (2013).
- [31] S. Datta, *Electronic transport in mesoscopic systems* (Cambridge university press, 1997).
- [32] O. Klein, Die reflexion von elektronen an einem potentialsprung nach der relativistischen dynamik von dirac, *Zeitschrift für Physik* **53**, 157 (1929).
- [33] C. W. J. Beenakker, Colloquium: Andreev reflection and klein tunneling in graphene, *Rev. Mod. Phys.* **80**, 1337 (2008).
- [34] S. Lee, V. Stanev, X. Zhang, D. Stasak, J. Flowers, J. S. Higgins, S. Dai, T. Blum, X. Pan, V. M. Yakovenko, *et al.*, Perfect andreev reflection due to the klein paradox in a topological superconducting state, *Nature* **570**, 344 (2019).
- [35] P. Adroguer, C. Grenier, D. Carpentier, J. Cayssol, P. Degiovanni, and E. Orignac, Probing the helical edge states of a topological insulator by cooper-pair injection, *Phys. Rev. B* **82**, 081303 (2010).
- [36] A. M. Zagoskin, *Quantum theory of many-body systems*, Vol. 174 (Springer, 1998).
- [37] C. Beenakker, Three “universal” mesoscopic josephson effects, in *Transport Phenomena in Mesoscopic Systems: Proceedings of the 14th Taniguchi Symposium, Shima, Japan, November 10–14, 1991* (Springer, 1992) pp. 235–253.
- [38] H.-J. Kwon, K. Sengupta, and V. M. Yakovenko, Fractional ac josephson effect in p-and d-wave superconductors, *The European Physical Journal B-Condensed Matter and Complex Systems* **37**, 349 (2004).
- [39] D. I. Pikulin and Y. V. Nazarov, Phenomenology and dynamics of a majorana josephson junction, *Phys. Rev. B* **86**, 140504 (2012).
- [40] M. Houzet, J. S. Meyer, D. M. Badiane, and L. I. Glazman, Dynamics of majorana states in a topological josephson junction, *Phys. Rev. Lett.* **111**, 046401 (2013).
- [41] I. O. Kulik and A. N. Omel'yanchuk, Josephson effect in superconductive bridges: microscopic theory, *Soviet Journal Low Temperature Physics* **4**, 142 (1978).
- [42] R. Arouca, J. Cayao, and A. M. Black-Schaffer, Topological superconductivity enhanced by exceptional points, *Phys. Rev. B* **108**, L060506 (2023).
- [43] L. Maier, J. B. Oostinga, D. Knott, C. Brüne, P. Virtanen, G. Tkachov, E. M. Hankiewicz, C. Gould, H. Buhmann, and L. W. Molenkamp, Induced superconductivity in the three-dimensional topological insulator hgte, *Phys. Rev. Lett.* **109**, 186806 (2012).
- [44] V. S. Stolyarov, D. Roditchev, V. L. Gurtovoi, S. N. Kozlov, D. S. Yakovlev, O. V. Skryabina, V. M. Vinokur, and A. A. Golubov, Resonant oscillations of josephson current in Nb-Bi<sub>2</sub>Te<sub>2.3</sub>Se<sub>0.7</sub>-Nb junctions, *Advanced Quantum Technologies* **5** (2022).
- [45] S. Charpentier, L. Galletti, G. Kunakova, R. Arpaia, Y. Song, R. Baghdadi, S. M. Wang, A. Kalaboukhov, E. Olsson, F. Tafuri, *et al.*, Induced unconventional superconductivity on the surface states of bi<sub>2</sub>te<sub>3</sub> topological insulator, *Nature Communications* **8**, 2019 (2017).
- [46] F. Roccati, G. M. Palma, F. Ciccarello, and F. Bagarello, Non-hermitian physics and master equations, *Open Systems & Information Dynamics* **29**, 2250004 (2022).
- [47] D. Manzano, A short introduction to the Lindblad master equation, *AIP Advances* **10**, 025106 (2020).